Opto-Electronics Review 33 (2025) e154201

Opto-Electronics Review

journal homepage: https://journals.pan.pl/opelre

Theoretical investigation and numerical simulation of gas-filled multi-pass cell

Haotian Shi[1,2], Yani Zuo[2], Fangfei Wu[1], Huifeng Zheng[1], Chenghua Sui[3], Xiaoyue Wang[1*]

[1] China Jiliang University, Hangzhou, China
[2] Division of Time and Frequency Metrology, National Institute of Metrology (NIM), Beijing, China
[3] YIXI Intelligent Technology (YIXIST) Co., Ltd., Hangzhou, Zhejiang, China

Article info

Article history:
Received 13 Feb. 2025
Received in revised form 10 Mar. 2025
Accepted 10 Mar. 2025
Available on-line 26 Mar. 2025

Keywords:
multi-pass cell;
eigenmode;
beam evolution;
ABCD transfer matrix.

Abstract

Gas-filled multi-pass cell (MPC) has been widely used in physics and optics studies. An important issue that cannot be ignored is the instability of beam propagation, which will destroy the optical elements and weaken the experimental performance. In this paper, the authors propose a theoretical investigation of MPC, not only the analytical solution of the eigenmode, but also the beam evolution in gas-filled MPC. Based on the symmetrical configuration of MPC, the model is established using the ABCD matrix method and the beam transmission evolution in MPC. The analytical eigenmode solution is derived by solving the functions of q-parameter transformation. The beam size and wavefront radius verify the correctness of the eigenmode. Then, the transfer matrix calculates the beam evolution of 100 passes in MPC. Compared to the traditional eigenmode calculation, the method proposed in this paper has higher stability. Starting from a theoretical perspective, this paper addresses the issue of an unstable beam transmission in MPC, which is significant for designing and evaluating MPC configuration in frontier scientific research.

1. Introduction

Driven by the needs of frontier research, a gas-filled multi-pass cell (MPC) technique has rapidly developed [1]. MPC has been widely used in studies and applications, including quantum physics [2, 3], spectroscopy [4–6], ultrafast optics [7–9], and interferometry [10–12]. An MPC structure contains two concave reflective mirrors, resembling a resonant cavity. Based on this structure, the beam can transmit back and forth multiple times in the MPC cavity. By increasing the optical path length, several advantages can be achieved, such as obtaining optical delay, enhancing quantum effects, and strengthening nonlinear effects [13, 14]. At the same time, based on the symmetry configuration as a resonator, with the eigenmode condition, the beam propagates stably in the MPC and the laser output from the MPC has high beam quality [15]. Therefore, the two main advantages of the MPC are increasing the optical path length of the laser and maintaining beam quality.

MPC has a portable structure that can effectively extend the optical path length while maintaining beam quality, making it widely used in research. In spectroscopy and gas detection, Yang *et al.* proposed a miniaturized MPC to measure O_2 concentration [16]. A miniaturized MPC was developed to suppress the interference of ambient O_2 and a minimum detection sensitivity was 0.05% in an integration time of 141 s. Based on an MPC compact spherical mirror, Fang *et al.* proposed a portable formaldehyde sensor for laser spectroscopy [17]. It has a high fill factor, providing a 350 mL sampling volume and a 50.6 m optical path length, providing a minimum detection absorption coefficient of 2.3×10^{-9} cm^{-1}. In quantum physics, aiming to measure weak fields, Liu *et al.* provided a high-sensitivity atomic vector magnetometer based on orthogonal MPCs [18]. The magnetic field sensitivities at three axes were all better than 85 fT/Hz$^{1/2}$ at a bandwidth of 0.1 Hz. Its stability was better than 1.5 pT during a long integration time of 10^4 s. Based on MPC techniques, this magnetometer made an attractive step for a long-term stable detection of weak fields. Yi *et al.* proposed an MPC-assisted free-induction-decay ^{4}He magnetometer [19]. Based on the

*Corresponding author at: xywang_phy@163.com

https://doi.org/10.24425/opelre.2025.154201
1896-3757/ Association of Polish Electrical Engineers (SEP) and Polish Academic of Sciences (PAS). Published by PAS

MPC structure, it not only had the advantages of a high bandwidth of 5 kHz, but also maintained high sensitivity with a magnetic field floor of 0.34 pT/Hz$^{1/2}$. In the field of ultra-fast and ultra-intense optics, Kaumanns *et al.* proposed an MPC configuration for spectral broadening and the pulse width was compressed from 1.3 ps to 37 fs [20]. It also conserved an excellent spatial spectral homogeneity of ~98%. Müller *et al*. proposed a 2-stage MPCs configuration and a dispersion compensation system was used between two MPCs. The pulse width was compressed to 6.9 fs from a 200 fs initial width. This work demonstrated a helpful method to obtain high-power and few-cycle laser pulses.

Thanks to the advantages of MPC, research in several cutting-edge disciplines has yielded significant results. However, in actual experiments, an urgent issue exists regarding the instability of beam propagation during the MPC transmission [13, 21–26]. It can be observed that the beam size varies each time it travels at a certain location in the MPC. Due to the resonator theory, similar to the resonator cavity, the MPC also has a symmetrical configuration. Thus, an eigenmode can propagate stably in the MPC [27, 28]. The unstable propagation is caused by mode-mismatching between the input beam mode and the MPC eigenmode. The eigenmode calculation does not consider the refractive index. It can be noticed that the refractive index of the gas changes with the gas pressure [29]. Substituting the MPC eigenmode with a traditional resonator eigenmode calculation will cause severe errors. A mismatching mode will cause unstable transmission during tens or hundreds of propagations in MPC. A small beam size may cause a high intensity that exceeds the damage threshold, destroying the optical components in MPC. A large beam size will shorten quantum effects, nonlinear effects, or spectral absorption which weaken the experimental performance. Thus, obtaining the precise eigenmode and the beam evolution in the MPC is crucial.

In this paper, the authors propose a theoretical investigation of a gas-filled MPC, aiming to solve the instability of beam propagation in MPC. First, the authors organize and arrange the ABCD matrix of each optical component and the whole optical system of MPC [30, 31]. Then, based on the symmetrical configuration, a consistency relationship is established by changing the q-parameter. The analytical solution of the MPC eigenmode is derived by solving these formulas considering the gas refractive index. The beam radius and wavefront radius verify the correctness of the eigenmode in the passes in the MPC. Then, the authors conduct numerical simulations of the beam evolutions during 100 passes in the gas-filled MPC. Compared to the input beam with the mode calculated by the resonator eigenmode, the authors' method has higher transmission stability in the MPC. This paper proposes a valuable theoretical insight into the gas-filled MPC and provides the analytical solution of the eigenmode, demonstrating helpful designs and evaluation for the MPC configurations in various studies, including quantum physics, spectroscopy, ultra-fast optics, and interferometry.

2. Theory

This section describes the gas-filled MPC model and its eigenmode, as well as beam propagation characteristics. First, based on the MPC structure, the ABCD matrix of each optical element and the total optical system are introduced. Then, using the properties of the q-parameter during beam propagation, an analytical solution for the eigenmode can be obtained. After obtaining the eigenmode, the beam size and wavefront curvature radius at any location within the MPC can be determined using the ABCD matrix.

2.1. ABCD matrix method

Figure 1(a) shows the MPC configuration. Two planar reflective mirrors (RM1 and RM2) are used to let the beam inject in and get out from the MPC. It comprises two facing concave reflective mirrors (CM1 and CM2) with the same curvature as R_{CM}. The distance between CM1 and CM2 is L filled with gas. Laser beams will transmit repetitively between these two concave mirrors by reflections. Figure 1(b) demonstrates the paraxial approximation of the MPC. These two concave mirrors are substituted with a series of thin lenses, with the focal length $f = R_{CM}/2$. The distance between two adjacent thin lenses is L, with gas between them.

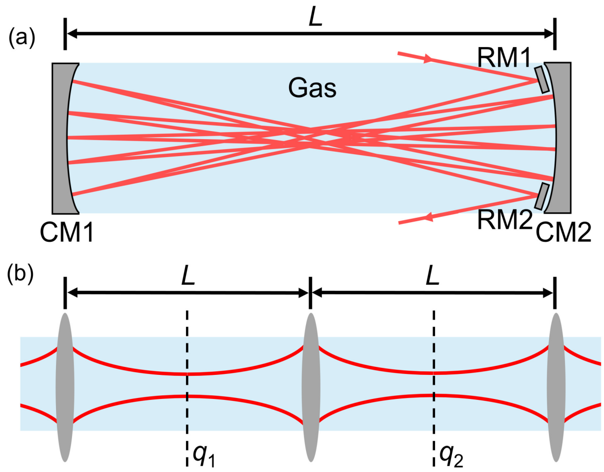

Fig. 1. (a) Schematic diagram of MPC. (b) Paraxial approximation of MPC.

With the paraxial approximation condition, the ABCD matrix of a concave mirror is as follows:

$$M_{CM} = \begin{bmatrix} 1 & 0 \\ -2/R_{CM} & 1 \end{bmatrix}. \tag{1}$$

The ABCD matrix of the propagation distance of l in gas is:

$$M_l = \begin{bmatrix} 1 & l \\ 0 & 1 \end{bmatrix}. \tag{2}$$

Based on (1) and (2), for a beam starting from the centre of MPC, passing through $L/2$ in the gas, reflecting from a concave mirror, and then passing through another $L/2$ in the gas, the ABCD matrix of this optical system is:

$$\begin{aligned} M_1 &= M_{L/2} M_{\mathrm{CM}} M_{L/2} \\ &= \begin{bmatrix} 1 & L/2 \\ 0 & 1 \end{bmatrix} \begin{bmatrix} 1 & 0 \\ -2/R_{\mathrm{CM}} & 1 \end{bmatrix} \begin{bmatrix} 1 & L/2 \\ 0 & 1 \end{bmatrix} \\ &= \begin{bmatrix} A_1 & B_1 \\ C_1 & D_1 \end{bmatrix}. \end{aligned} \tag{3}$$

For a beam starting from the mirror surface, passing through L in the gas and reflecting from a concave mirror, the ABCD matrix of such an optical system is:

$$\begin{aligned} M_2 &= M_{\mathrm{CM}} M_L \\ &= \begin{bmatrix} 1 & 0 \\ -2/R_{\mathrm{CM}} & 1 \end{bmatrix} \begin{bmatrix} 1 & L \\ 0 & 1 \end{bmatrix} \\ &= \begin{bmatrix} A_2 & B_2 \\ C_2 & D_2 \end{bmatrix}. \end{aligned} \tag{4}$$

In (3) and (4), the determinant has the relation of:

$$\det M = AD - BC = 1. \tag{5}$$

2.2. Gas-filled MPC model

In the paraxial approximation, the q-parameter is used to describe a Gaussian beam which is expressed as:

$$\frac{1}{q} = \frac{1}{R} - i\frac{\lambda}{\pi n \omega^2}, \tag{6}$$

where R is the curvature of the wavefront, λ is the wavelength, n is the refractive index, ω is the beam radius.

In Fig. 1(b), if a Gaussian beam propagates from the centre of the MPC with a q-parameter equal to q_1 after transmitting a single pass in the MPC, it has the q-parameter equal to q_2. The relation between q_1 and q_2 is as follows:

$$q_2 = \frac{A_1 q_1 + B_1}{C_1 q_1 + D_1}. \tag{7}$$

Due to the resonator theory, if the beam satisfies the eigenmode condition, the beam will be stable during transmission in the cavity, thus:

$$q_2 = q_1. \tag{8}$$

By solving (6) to (8), for a gas-filled MPC, the theoretical solution of the eigenmode in the centre of the MPC is:

$$\omega_c = \left(\frac{\lambda}{2n\pi} \left(L(2R - L) \right)^{1/2} \right)^{1/2}. \tag{9}$$

Using a similar method, the theoretical solution of the eigenmode on the mirror surface is:

$$\omega_m = \left(\frac{\lambda R}{n\pi} \left(\frac{2R}{L} - 1 \right)^{1/2} \right)^{1/2}. \tag{10}$$

After getting the MPC eigenvalues, the beam evolution of any position in the MPC can be calculated based on the combination and arrangement of (1) and (2).

3. Results and discussions

In this section, the authors conduct a simulation with the gas-filled MPC model proposed in this paper. The wavefront radius in the MPC centre and on the concave mirror verifies the correctness of the eigenmode. The beam evolution of the gas-filled MPC model is compared with that of the traditional resonator model.

The first part of the numerical calculation is the eigenmode. A gas-filled MPC configuration of $L = 995$ mm and $R = 500$ mm is used, with a gas refractive index of 1.05 and an input beam with a centre wavelength of 1064 nm. Based on (9) and (10), the eigenmode sizes in the centre and that on the mirror are calculated as $\omega_c = 0.1067$ mm and $\omega_m = 1.5083$ mm.

According to the resonator theory, these eigenvalues with their theoretical wavefront radii of ∞ and 500 mm are put into the gas-filled MPC model to verify the correctness. For each time, the beam propagates in the MPC centre, its beam radius and wavefront radius are depicted as the red curves in Fig. 2(a) and (b). The red curves in Fig. 2(c) and (d) show its beam and wavefront radius evolution when it travels on the mirror surface. It is observed that the evolution of beam radii in the MPC centre and on the mirror is stable. Furthermore, the curvature of the wavefront in each pass is of the order of 10^{14} m or 10^{15} m. The wavefront is a plane in the MPC centre and when it propagates on the concave mirror, it matches the curvature of the mirror surface. In summary, the authors analyse the beam size and wavefront in the MPC, demonstrating the correctness of the eigenvalue calculation method proposed in this paper.

Then, the authors compared the input beam with the mode calculated by the traditional resonator method, with $\omega_{c1} = 0.1067$ mm and $\omega_{m1} = 1.5456$ mm, shown as the blue curves in Fig. 2(a) to (d). The beam radii are unstable in the centre and on the mirror. The wavefronts are also distorted. This phenomenon is due to the mode-mismatching of the MPC configuration. The eigenmode calculation from the traditional resonator model should be cautious in the estimation of the input beam in the gas-filled MPC.

During each trip in the gas-filled MPC, with eigenmode condition, the beam radius and wavefront evolutions are shown as the red curves and green curves in Fig. 3. The beam sizes on the two mirrors are the same, with a radius of 1.5083 mm. The beam radius gets a minimum value of 0.1067 mm in the centre. The wavefront radius also has a symmetry scheme where the plus or minus signs mean the bending direction of the wavefront.

Furthermore, the authors simulate the evolutions of the beam and wavefront radius during 100 passes in the gas-filled MPC, with the input beam mode calculated by the gas-filled MPC model proposed in this paper and the traditional resonator model. The propagation step is 1 mm. For the input beam with the mode calculated by the

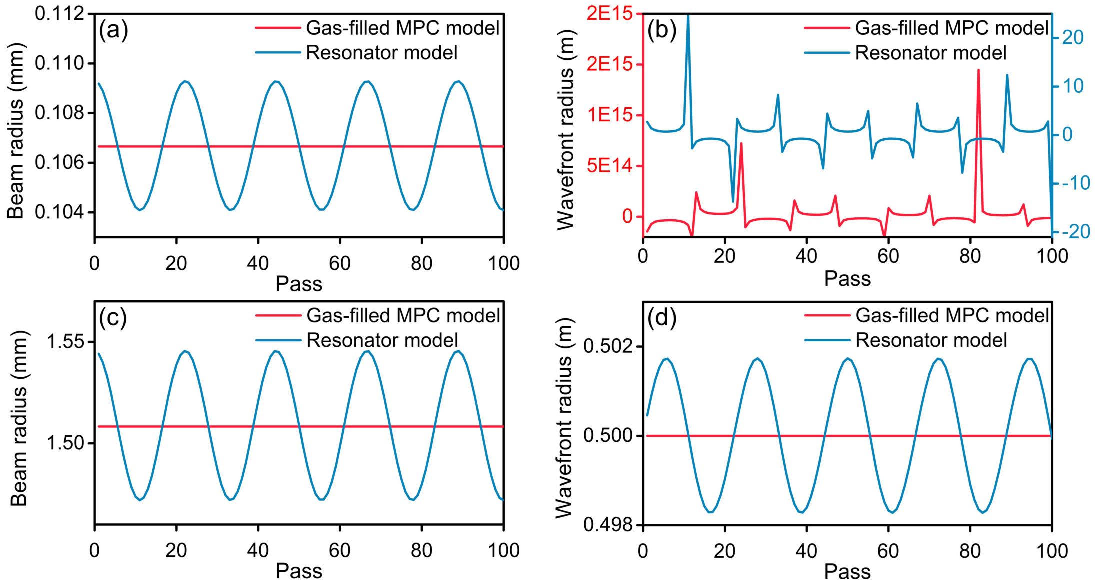

Fig. 2. In the MPC centre: (a) beam radius, (b) wavefront radius. On the concave mirror: (c) beam radius, (d) wavefront radius.

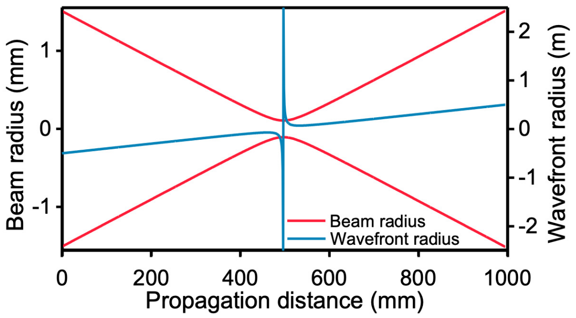

Fig. 3. Beam radius and wavefront evolutions during a single trip in gas-filled MPC.

gas-filled MPC and traditional resonator models, the evolutions are depicted in Fig. 4(a) and (b). The wavefront radius evolutions simulated by these two methods are shown in Fig. 4(c) and (d). In Fig. 4(a) and (c), each row shows the beam size and wavefront evolution in the MPC, and each row is the same, which meets the eigenmode condition in the cavity. The inclination of the surface in Fig. 4(c) indicates the variation trend in the degree of wavefront curvature. However, using the input mode calculated by the traditional resonator method is shown in Fig. 4(b) and (d). The beam size evolution has the characteristics of fluctuation and instability and the wavefront curvature becomes unstable each time it passes through the gas-filled MPC. These four subfigures in Fig. 4

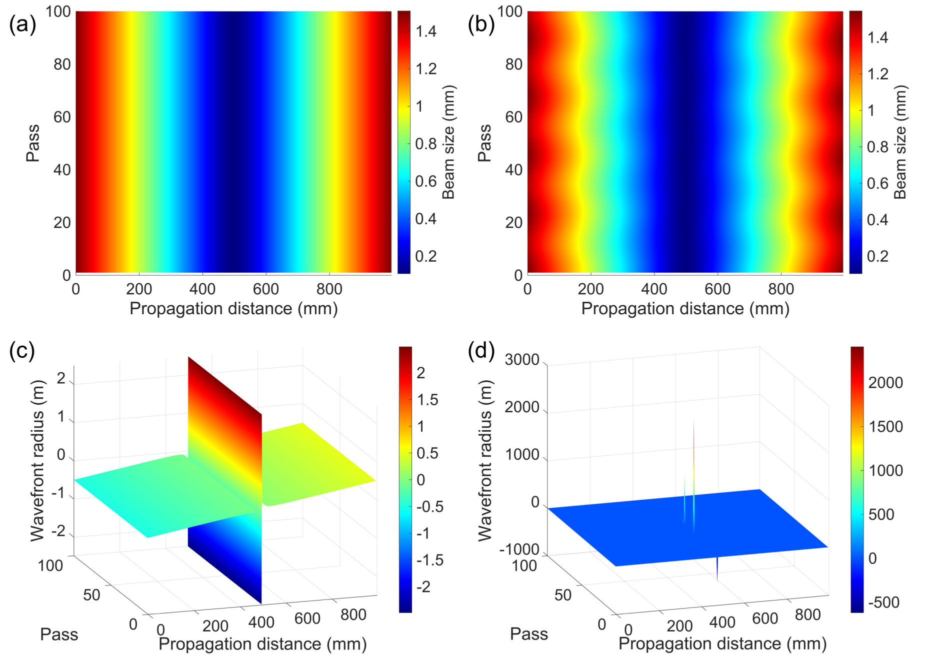

Fig. 4. Beam radius evolution with: (a) gas-filled MPC model, (b) resonator model. Wavefront radius evolution with: (c) gas-filled MPC model, (d) resonator model.

also demonstrate the correctness and reliability of the gas-filled MPC model proposed in this paper and the beam evolution in each position in the cavity can be obtained.

In this section, the authors calculate the eigenmode and simulation of the beam evolution. They also verify the correctness of this model by the radius and wavefront radius in the MPC centre and on the mirror. The results show that if the input beam has only a few micrometers or tens of micrometers of difference from the eigenvalue, heavy fluctuations will appear, which is harmful to the experiment. Thus, the gas-filled MPC model proposed in this paper is helpful in the design and evaluation of the MPC configuration in various optical and quantum physical experiments.

4. Conclusions

In this paper, the authors proposed a gas-filled MPC model to obtain the analytical solution of eigenmodes and get the beam evolution, aiming to solve the instability of beam transmission within the gas-filled MPC in the field of ultra-fast optics and quantum physics. The model is established based on the ABCD matrix method and q-parameter characteristics in the MPC. Then, the analytical eigenmodes of the gas-filled MPC are derived. The correctness of this method is verified by the values of beam radius and wavefront radius in the MPC centre and on the concave mirror. After that, the authors simulate beam evolution during 100 passes transmitting in the MPC. The stability of the eigenmode calculated by the method proposed in this paper is much steadier than the mode with the traditional method. As such, the gas-filled MPC model, as well as the analytical solution of the eigenmode, can help design and evaluate MPC configurations. It could also be extended to enhance the nonlinear effects in ultrafast optics and increase the detection precision in quantum precise measurements.

Authors' statement

Design, data analysis, writing the article, H.S.; research concept, interpretation, Y.Z. and F.W.; collection and assembly of data, H.Z. and C.S.; critical revision, final approval of article, X.W.

Acknowledgements

This work was supported by the National Key R&D Program of China (Grant No. 2021YFF0603800), National Natural Science Foundation of China (Grant No. 1230030120), the Natural Science Foundation of Zhejiang Province (Grant No. LQ24A040005, LQ24F050006), and the Fundamental Research Funds for the Provincial Universities of Zhejiang (Grant No. 2023YW54, 2023YW62).

References

[1] Shcherbakova, A. V. *et al*. Experimental setup based on a quantum cascade laser tunable in the wavelength range of 5.3–12.8 μm for spectral analysis of human exhaled air. *Opt. Spectrosc*. **129**, 830–837 (2021). https://doi.org/10.1134/S0030400X21060151

[2] Lucivero, V. G., Lee, W., Dural, N. & Romalis, M. V. Femtotesla direct magnetic gradiometer using a single multipass cell. *Phys. Rev. Appl.* **15**, 014004 (2021). https://doi.org/10.1103/PhysRevApplied.15.014004

[3] Cai, B. *et al.* Herriott-cavity-assisted all-optical atomic vector magnetometer. *Phys. Rev. A* **101**, 053436 (2020). https://doi.org/10.1103/PhysRevA.101.053436

[4] Wang, R. *et al.* Double-enhanced multipass cell-based wavelength modulation spectroscopy CH_4 sensor for ecological applications. *Opt. Express* **31**, 3237–3248 (2023). https://doi.org/10.1364/OE.480496

[5] Wang, L. *et al.* Enhanced photoacoustic spectroscopy integrated with a multi-pass cell for ppb level measurement of methane. A*ppl. Sci.* **14**, 6068 (2024). https://doi.org/10.3390/app14146068

[6] Hudzikowski, A., Głuszek, A., Krzempek, K. & Sotor, J. Compact, spherical mirror-based dense astigmatic-like pattern multipass cell design aided by a genetic algorithm. *Opt. Express* **29**, 26127–26136 (2021). https://doi.org/10.1364/OE.432541

[7] Omar, A., Vogel, T., Hoffmann, M. & Saraceno, C. J. Spectral broadening of 2-mJ femtosecond pulses in a compact air-filled convex–concave multi-pass cell. *Opt. Lett.* **48**, 1458–1461 (2023). https://doi.org/10.1364/OL.481774

[8] Graf, M., Emmenegger, L. & Tuzson, B. Compact, circular, and optically stable multipass cell for mobile laser absorption spectroscopy. *Opt. Lett*. **43**, 2434–2437 (2018). https://doi.org/10.1364/OL.43.002434

[9] Roberts, F. C., Lewandowski, H. J., Hobson, B. F. & Lehman, J. H. A rapid, spatially dispersive frequency comb spectrograph aimed at gas phase chemical reaction kinetics. *Mol. Phys*. **118**, e1733116 (2020). https://doi.org/10.1080/00268976.2020.1733116

[10] Gao, B., Wu, T. & Zhou, Q. Optimization of air refractive index based on dispersive interferometry, *Opt. Express* **32**, 27958–27973 (2024). https://doi.org/10.1364/OE.530417

[11] Cheng, G., Cao, Y.-N., Tian, X., Chen, J.-J. & Wang, J.-J. Design and analysis of novel folded optical multi-pass cell. *Front. Phys.* **10**, 907715 (2022). https://doi.org/10.3389/fphy.2022.907715

[12] Mikkonen, T., Hieta, T., Genty, G. & Toivonen, J. Sensitive multi-species photoacoustic gas detection based on mid-infrared supercontinuum source and miniature multipass cell. *Phys. Chem. Chem. Phys.* **24**, 19481–19487 (2022). https://doi.org/10.1039/D2CP01731H

[13] Daher, N. *et al*. Multipass cells: 1D numerical model and investigation of spatio-spectral couplings at high nonlinearity *J. Opt. Soc. Am. B* **37**, 993–999 (2020). https://doi.org/10.1364/JOSAB.386049

[14] Cao, Y. *et al*. The design and simulation of a novel ring multi-pass optical cell for detection of environmental trace gas. *Optik* **227**, 166095 (2021). https://doi.org/10.1016/j.ijleo.2020.166095

[15] Viotti, A.-L. *et al.* Multi-pass cells for post-compression of ultrashort laser pulses. *Optica* **9**, 197–216 (2022). https://doi.org/10.1364/OPTICA.449225

[16] Yang, T. *et al*. A miniaturized multipass cell for measurement of O_2 concentration in vials based on TDLAS. *Opt. Lasers Eng*. **163,** 107454 (2023). https://doi.org/10.1016/j.optlaseng.2022.107454

[17] Fang, B. *et al*. Highly sensitive portable laser absorption spectroscopy formaldehyde sensor using compact spherical mirror multi-pass cell. *Sens. Actuators B Chem.* **394**, 134379 (2023). https://doi.org/10.1016/j.snb.2023.134379

[18] Liu, S.-Q., Yu, Q.-Q., Zhou, H. & Sheng, D. Sensitive and stable atomic vector magnetometer to detect weak fields using two orthogonal multipass cavities. *Phys. Rev. Appl.* **19**, 044062 (2023). https://doi.org/10.1103/PhysRevApplied.19.044062

[19] Yi, K. *et al.* Free-induction-decay ^{4}He magnetometer using a multipass cell. *Phys. Rev. Appl.* **22**, 014084 (2024). https://doi.org/10.1103/PhysRevApplied.22.014084

[20] Kaumanns, M., Kormin, D., Nubbemeyer, T., Pervak, V. & Karsch, S. Spectral broadening of 112 mJ, 1.3 ps pulses at 5 kHz in a LG_{10} multipass cell with compressibility to 37 fs. *Opt. Lett*. **46**, 929–932 (2021). https://doi.org/10.1364/OL.416734

[21] Kaur, J. *et al*. Simultaneous nonlinear spectral broadening and temporal contrast enhancement of ultrashort pulses in a multi-pass cell. *J. Phys. Photonics* **6**, 015001 (2024). https://doi.org/10.1088/2515-7647/ad078a

[22] Segundo, V. W. *et al*. Numerical investigation of gas-filled multipass cells in the enhanced dispersion regime for clean spectral

broadening and pulse compression. *Opt. Express* **31**, 18898–18906 (2023). https://doi.org/10.1364/OE.481054

[23] Kong, R., Sun, T., Liu, P. & Zhou, X. Optical design and analysis of a two-spherical-mirror-based multipass cell. *Appl. Opt.* **59**, 1545–1562 (2020). https://doi.org/10.1364/AO.381632

[24] Webster, C. R., Flesch, G. J., Briggs, R. M., Fradet, M. & Christensen, L. E. Herriott cell spot imaging increases the performance of tunable laser spectrometers. *Appl. Opt.* **60**, 1958–1965 (2021). https://doi.org/10.1364/AO.417074

[25] Hanna, M., Daher, N., Guichard, F., Délen, X. & Georges, P. Hybrid pulse propagation model and quasi-phase-matched four-wave mixing in multipass cells. *J. Opt. Soc. Am. B* **37**, 2982–2988 (2020). https://doi.org/10.1364/JOSAB.395789

[26] Zhang, B. *et al.* High-sensitivity photoacoustic gas detector by employing multi-pass cell and fiber-optic microphone. *Opt. Express* **28**, 6618–6630 (2020). https://doi.org/10.1364/OE.382310

[27] Kogelnik, H. & Li, T. Laser beams and resonators. *Appl. Opt.* **5**, 1550–1567 (1966). https://doi.org/10.1364/AO.5.001550

[28] Herriott, D., Kogelnik, H. & Kompfner, R. Off-axis paths in spherical mirror interferometers. *Appl. Opt.* **3**, 523–526 (1964). https://doi.org/10.1364/AO.3.000523

[29] Schuurmans, F. J. P., de Lang, D. T. N., Wegdam G. H., Sprik, R. & Lagendijk, A. Local-field effects on spontaneous emission in a dense supercritical gas. *Phys. Rev. Lett.* **80**, 5077–5080 (1998). https://doi.org/10.1103/PhysRevLett.80.5077

[30] Martin-Sanchez, D. *et al.* ABCD transfer matrix model of Gaussian beam propagation in Fabry-Perot etalons. *Opt. Express* **30**, 46404–46417 (2022). https://doi.org/10.1364/OE.477563

[31] Martin-Sanchez, D., Li, J., Zhang, E. Z., Beard, P. C. & Guggenheim, J. A. ABCD transfer matrix model of Gaussian beam propagation in plano-concave optical microresonators. *Opt. Express* **31**, 16523–16534 (2023). https://doi.org/10.1364/OE.484212